

The Wnt Co-receptor LRP5 Is Essential for Skeletal Mechanotransduction but Not for the Anabolic Bone Response to Parathyroid Hormone Treatment*

Received for publication, February 1, 2006, and in revised form, April 25, 2006 Published, JBC Papers in Press, June 20, 2006, DOI 10.1074/jbc.M601000200

Kimihiko Sawakami[†], Alexander G. Robling[§], Minrong Ai[¶], Nathaniel D. Pitner[‡], Dawei Liu[‡], Stuart J. Warden[‡], Jiliang Li[§], Peter Maye^{||}, David W. Rowe^{||}, Randall L. Duncan[‡], Matthew L. Warman[¶], and Charles H. Turner^{†‡}

From the [†]Department of Orthopedic Surgery, Biomechanics and Biomaterials Research Center, and the [§]Department of Anatomy & Cell Biology, Indiana University School of Medicine, Indianapolis, Indiana 46202, the [¶]Howard Hughes Medical Institute and Department of Genetics and Center for Human Genetics, Case School of Medicine and University Hospitals of Cleveland, Cleveland, Ohio, 44106 and the ^{||}Department of Genetics and Developmental Biology, University of Connecticut Health Center, Farmington, Connecticut 06030

The cell surface receptor, low-density lipoprotein receptor-related protein 5 (LRP5) is a key regulator of bone mass. Loss-of-function mutations in LRP5 cause the human skeletal disease osteoporosis-pseudoglioma syndrome, an autosomal recessive disorder characterized by severely reduced bone mass and strength. We investigated the role of LRP5 on bone strength using mice engineered with a loss-of-function mutation in the gene. We then tested whether the osteogenic response to mechanical loading was affected by the loss of Lrp5 signaling. Lrp5-null ($Lrp5^{-/-}$) mice exhibited significantly lower bone mineral density and decreased strength. The osteogenic response to mechanical loading of the ulna was reduced by 88 to 99% in $Lrp5^{-/-}$ mice, yet osteoblast recruitment and/or activation at mechanically strained surfaces was normal. Subsequent experiments demonstrated an inability of $Lrp5^{-/-}$ osteoblasts to synthesize the bone matrix protein osteopontin after a mechanical stimulus. We then tested whether $Lrp5^{-/-}$ mice increased bone formation in response to intermittent parathyroid hormone (PTH), a known anabolic treatment. A 4-week course of intermittent PTH (40 μ g/kg/day; 5 days/week) enhanced skeletal mass equally in $Lrp5^{-/-}$ and $Lrp5^{+/+}$ mice, suggesting that the anabolic effects of PTH do not require Lrp5 signaling. We conclude that Lrp5 is critical for mechanotransduction in osteoblasts. Lrp5 is a mediator of mature osteoblast function following loading. Our data suggest an important component of the skeletal fragility phenotype in individuals affected with osteoporosis-pseudoglioma is inadequate processing of signals derived from mechanical stimulation and that PTH might be an effective treatment for improving bone mass in these patients.

Low-density lipoprotein receptor-related protein 5 (LRP5)² is a single-pass transmembrane protein that functions as a co-receptor for the secreted family of Wnt glycoproteins (1). Wnt signaling, particularly through LRP5, is emerging as a key pathway in the regulation of bone mass and strength. For example, the autosomal recessive human disease osteoporosis-pseudoglioma syndrome (OPPG) is caused by loss-of-function mutations in LRP5 (2). Patients with OPPG present with bone mineral densities (BMD) several standard deviations below the mean and are prone to skeletal fracture and deformity. Interestingly, heterozygous carriers of loss-of-function mutations have mean BMDs in the osteoporotic range, indicating a dose-dependent effect of LRP5 function (2). Conversely, single amino acid missense mutations in LRP5, which alter the ability of the receptor to be regulated by endogenous inhibitors (3–5), segregate with an abnormally high bone mass phenotypes in an autosomal dominant manner (6–8). Affected individuals have BMD values that are several standard deviations above the mean and have increased bone strength.

In addition to studies in humans, mice have been created with loss-of-function mutations in the mouse ortholog of LRP5, called Lrp5 (9–11). These mice recapitulate the clinical features observed in OPPG patients, suggesting that the mouse is a useful animal model for delineating the role of Lrp5 in the mammalian skeleton (9–11). Additionally, transgenic mice that overexpress wild-type Lrp5 or a high bone mass causing missense allele of LRP5 (G171V) under control of the type I collagen promoter, have increased bone mass and skeletal strength (12). Taken together, these data indicate that LRP5 has an important role in determining skeletal mass, strength, and function.

Although loss-of-function mutations in LRP5 impart clear deficiencies on the skeleton, it is unclear how LRP5 participates in the modulation of bone mass. The striking similarity between

* This work was supported by National Institutes of Health Grants AR046530 (to C. H. T.) and AR053237 (to A. G. R.). The costs of publication of this article were defrayed in part by the payment of page charges. This article must therefore be hereby marked "advertisement" in accordance with 18 U.S.C. Section 1734 solely to indicate this fact.

[†] To whom correspondence should be addressed: Indiana University School of Medicine, 1120 South Dr., FH 115, Indianapolis, IN 46202. Tel.: 317-274-3226; Fax: 317-274-3702; E-mail: turnerch@iupui.edu.

² The abbreviations used are: LRP5, low density lipoprotein receptor-related protein 5; OPPG, osteoporosis-pseudoglioma; BMD, bone mineral densities; PTH, parathyroid hormone; GFP, green fluorescent protein; BMC, bone mineral content; μ CT, microcomputed tomography; pQCT, peripheral quantitative computed tomography; MAPK, mitogen-activated protein kinase; N, newton; FSS, fluid shear stress; PGE₂, prostaglandin E₂; ERK, extracellular signal-regulated kinase; MS, mineralizing surface; BS, bone surface; MAR, mineral apposition rate; BFR, bone formation rate.

the OPPG skeletal phenotype and a mechanical disuse phenotype, whereby exposure of the skeleton to normal mechanical stresses and strains is limited, suggests that LRP5 might be involved in mechanotransduction signaling. For example, disuse induces a loss of trabecular bone volume (13, 14), a reduction in periosteal bone apposition (particularly when disuse occurs during growth) (15), and an increase in endocortical bone loss (particularly when disuse occurs during adulthood) (16). Biopsies and radiographic findings from patients with OPPG reveal reduced trabecular bone volume and reduced periosteal expansion (2, 17). The reduced trabecular bone volume is maintained at a normal turnover rate in OPPG patients, which is commonly observed in long term disuse conditions (15, 16). Moreover, mechanical stimulation of cultured osteoblasts causes translocation of β -catenin to the nucleus (18) and activation of a T cell factor responsive promoter (19), suggesting that mechanical loading activates canonical Wnt signaling.

We undertook an investigation of the role of Lrp5 in mechanical signaling. We hypothesized that Lrp5 modulates bone mass, size, and strength, and that one of the modes of action through which Lrp5 exerts its effects is mechanotransduction. To test our hypothesis, we generated knock-out mice in which Lrp5 was inactivated, and we subjected adult Lrp5^{-/-} mice to axial loading of the right ulna to stimulate osteogenesis *in vivo*. A nearly complete obliteration of an osteogenic response to *in vivo* loading was found in Lrp5^{-/-} mice. We then investigated the role of Lrp5 in modulating the anabolic response to parathyroid hormone (PTH) treatment and found that PTH remained equally effective in enhancing bone mass in Lrp5^{-/-} and Lrp5^{+/+} mice. The defect in mechanically induced osteogenesis was further investigated using an early osteoblast reporter mouse strain, which demonstrated that *in vivo* periosteal osteoblast recruitment/activation was not affected by Lrp5 deficiency. Studies of Lrp5^{-/-} and Lrp5^{+/+} primary osteoblasts *ex vivo* also indicated that loss of Lrp5 signaling appears to affect later stages in the mechanotransduction signaling cascade, such as matrix production, rather than the early sensing of mechanical strain. Our data indicate that Lrp5 signaling is not needed to respond to PTH treatment, but that Lrp5 is important for the ability of the skeleton to respond to mechanical loading.

EXPERIMENTAL PROCEDURES

Animals

Lrp5-deficient mice (Lrp5^{-/-}) were generated as reported previously (20). Briefly, the mice were created on a 129S/J background strain by disrupting exons 7 and 8 with a Lac-Z/Neo gene cassette. When correctly targeted, this allele does not express Lrp5 mRNA (Fig. 1), and produces no functional Lrp5 receptor, or receptor fragments. We interbred mice that were heterozygous carriers of this mutation and obtained wild-type (Lrp5^{+/+}), heterozygous (Lrp5^{+/-}), and homozygous mutant (Lrp5^{-/-}) offspring in the expected Mendelian genetic frequencies. To study osteoblast recruitment to mechanically strained surfaces after loading (see below), we bred the Lrp5 mutant allele onto the transgenic pOBCol3.6GFP mouse strain, in which green fluorescent protein (GFP) expression is driven

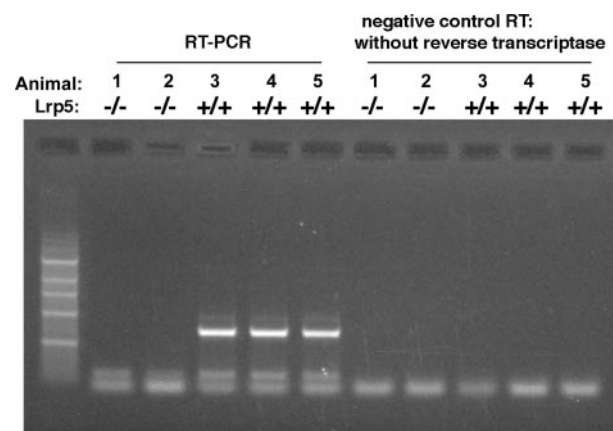


FIGURE 1. Loss of Lrp5 expression was confirmed in Lrp5^{-/-} mice by RT-PCR from RNA extracted from homogenized femurs and tibias of 5-week-old mice. Two Lrp5^{-/-} mice (mice 1 and 2) and 3 Lrp5^{+/+} mice (mice 3, 4, and 5) were used for expression confirmation. The 709-bp PCR product was evident in Lrp5^{+/+} but not Lrp5^{-/-} mice. Reactions run without enzyme (right lanes) showed no amplification in either genotype. RT, reverse transcriptase.

by the 3.6-kb rat type I collagen promoter fragment. The pOBCol3.6GFP mice exhibit strong expression of GFP in preosteoblasts and osteoblasts, with minimal to no GFP expression in other cell types (21). All procedures performed in the experiments were approved by the Institutional Animal Care and Use Committee guidelines where the animals were raised and studied.

Longitudinal *In Vivo* Peripheral Dual-energy X-ray Absorptiometry (pixiMUS)

Bone mineral content (BMC) of the whole body, spine, and femoral diaphysis were evaluated *in vivo* using peripheral dual-energy x-ray absorptiometry (pDXA; PIXImus II; GE-Lunar Corp., Madison, WI). Mice were anesthetized via inhalation of 2.5% isoflurane (IsoFlo; Abbott Laboratories, North Chicago, IL) mixed with O₂ (1.5 liter/min) for a total of ~8 min, including both induction and scanning. The mice were placed in prone position on a specimen tray and scanned. The head was excluded from total body scans. The region of interest for the spine included from the first lumbar vertebra (L1) to fifth lumbar vertebra (L5). The region of interest for the femur included the central 50% of the whole femur. We also analyzed hindlimb properties by positioning the region of interest box to include all skeletal tissue distal to the acetabulum. Scans were performed at 4, 8, 12, and 16 weeks of age (for the baseline phenotype characterization) or weekly from 12 to 16 weeks of age (for mice in PTH experiments; see below). All BMC measures were normalized by body weight to eliminate the confounding effects on changing body size and weight during growth.

Microcomputed Tomography (μ CT)

Geometric properties of femoral mid-diaphysis, trabecular bone volume fraction, and microarchitecture in the femoral distal metaphysis and L5 were evaluated using high-resolution desktop microcomputed tomography imaging systems (μ CT-20; Scanco Medical AG, Basserdorf, Switzerland). For geometric properties of the femoral shaft, a single transverse slice through the mid-diaphysis was taken at 9- μ m resolution. Each

Lrp5 in Bone Anabolic Pathways

mid-diaphysis slice was imported into Scion Image version 4.0.2 (Scion Corporation, Frederick, MD), in which the geometric properties were calculated using standard and customized macros. Geometric properties included cortical area (mm^2), and the maximum (I_{\max} , mm^4) and minimum (I_{\min} , mm^4) cross-sectional moments of inertia. In addition, we calculated polar moment of inertia I_p as the sum of I_{\max} and I_{\min} . The cross-sectional moment of inertia estimates the capacity of a beam (in this case, a bone diaphysis) to resist torsion and bending. For evaluation of the trabecular envelope at the femoral distal metaphysis and L5, each specimen was scanned with a slice increment of $9 \mu\text{m}$. CT images were reconstructed, filtered ($\sigma = 0.8$ and support = 1.0), and thresholded (22% of maximum possible gray scale value) as previously described (22). Scanning for the femur was started at 15% of the total femur length measured from the tip of femoral condyle and extended proximally for 100 slices. Scanning for the L5 vertebral body comprised 65% of the total vertebral body height, requiring ~ 200 slices through the central region. The area for trabecular analysis was outlined within the trabecular compartment, excluding the cortical and subcortical bone. Every 10 sections were outlined, and the intermediate sections were interpolated with the contouring algorithm to create a volume of interest. Parameters of microarchitecture for both skeletal sites included bone volume (BV, mm^3) and bone volume fraction (BV/TV, %), as well as trabecular number (Tb.N, mm^{-1}), trabecular thickness (Tb.Th, μm), and trabecular separation (Tb.Sp, μm). In addition, we computed the connectivity density (Conn.D, mm^{-3}) and structure model index (SMI), which indicates the platelike (SMI = 0) or rodlike (SMI = 3) nature of the underlying cancellous architecture.

Peripheral Quantitative Computed Tomography (pQCT)

The right femur of each mouse was analyzed for volumetric BMD (vBMD) using pQCT. Each femur was positioned in a plastic tube filled with 70% ethanol and centered in the gantry of a Norland Stratec XCT Research SA + pQCT (Stratec Electronics, Pforzheim, Germany). Using a collimation of 0.26 mm and a voxel size of 0.07 mm, three slices through the distal femur (15, 17.5, and 20% of the femoral length measured from the distal end of the femur) were recorded and averaged to obtain bone mineral measurements from a trabecular site. A single slice through the midshaft was also collected to monitor a cortical site.

Biomechanical Testing

Mechanical properties of the femur and L5 vertebra were tested as previously described (22). Briefly, femurs were brought to room temperature slowly (~ 2 h) in a saline bath and tested at the mid-diaphysis by three-point bending using a microforce materials testing machine (Vitrodyne V1000; Liveco, Inc., Burlington, VT). Load was applied in the antero-posterior direction midway between two supports positioned 9 mm apart. Tests were conducted at a cross-head speed of 0.2 mm/s , during which force and displacement were recorded at 0.025-s intervals. Load-displacement curves were generated, from which ultimate force (F_U ; N), stiffness (S ; N/mm), and work to failure (U ; mJ) were calculated. F_U represents the

strength of the bone, whereas U is a measure of the energy required to break the bone (23).

For L5, the end plates of the vertebral bodies were removed via parallel cuts on a diamond wafering saw (Isomet; Buehler, Lake Bluff, IL). After removing the neural arch by clipping through the pedicles, the vertebral bodies were submerged in a saline bath (~ 2 h) at room temperature and tested in axial compression at a cross-head speed of 0.05 mm/s . F_U , S , and U were calculated from the resulting load-displacement curves.

For *in situ* forearm mechanical testing, five mice at 16 weeks of age from each genotype were chosen at random. They were killed by cervical dislocation under isoflurane-induced anesthesia. The right forearm was stored in refrigerated 70% ethanol for later strain measurement. The left forearm was fixed between the cup-shaped platens and loaded to failure in compression at a cross-head speed of 2 mm/s . F_U was calculated from the resulting force *versus* displacement curves. The mean ultimate force calculated for each genotype was used to set three peak load magnitudes for the *in vivo* ulna loading experiments (see below).

In Vivo PTH Treatment

At 12 weeks of age, male and female $\text{Lrp5}^{-/-}$ and $\text{Lrp5}^{+/+}$ mice were administered subcutaneous injections of human PTH-(1–34) (40 $\mu\text{g}/\text{kg}$) or vehicle (99.7% normal saline, 0.2% bovine serum albumin, and 0.1% HCl) 5 day/week for 4 weeks. All animals in the PTH study were scanned using the pixiMUS densitometer at baseline (12 weeks) and at weekly intervals during the treatment (under isofluorane-induced anesthesia). Animals were sacrificed at 16 weeks of age, 1 day after their last PTH or vehicle injection.

In Vivo Ulna Loading

Male and female mice (16 weeks old) in each of the three genotypes were divided randomly into three load magnitude groups for *in vivo* loading ($n = 6$ –8/group) using the ulna loading protocol described by Torrance *et al.* (24). Under isofluorane-induced anesthesia, the right forearm of each mouse was loaded at 60 cycles/day for 3 consecutive days using a 2-Hz haversine waveform. Loading was applied using a previously described piezoelectric mechanical stimulator (25). The non-loaded left forearms served as an internal control. All mice were allowed normal cage activity between loading sessions. Intra-peritoneal injections of calcein (20 mg/kg body mass; Sigma) and alizarin (30 mg/kg body mass; Sigma) were administered 4 and 9 days after the first loading day. Animals were sacrificed 16 days after the first loading day.

Ulna Strain Measurements

The left forearms from mice used in the forearm testing group (described above) were brought to room temperature slowly (~ 2 h) in a saline bath and minimally dissected to expose the lateral surface of the mid-shaft ulna. A single element strain gauge (EA-06-015DJ-120; Measurements Group, Raleigh, NC) was bonded to the exposed medial ulnar surface at the midpoint of the ulna ($n = 5$ –6/group). The forearm was loaded in cyclic axial compression, using the loading device to be used for *in vivo* ulna loading. Using a 2-Hz haversine waveform, the

forearms were loaded at 1.0, 1.2, 1.4, 1.6, and 1.8 N, during which peak to peak voltage output from the strain gauge was measured on a digital oscilloscope. Voltage measurements were converted to strain as previously described (26). The strain gauged ulnae were scanned through the middle of the strain gauge on a μ CT at 9- μ m resolution. The mid-shaft slices were imported into Scion Image, wherein I_{\min} and the maximum section diameter in the I_{\min} plane (Se.Dm; mm) were calculated. From the geometric measurements and mechanical strain data, strain was estimated for the lateral periosteal surface of the histological sections from animals loaded *in vivo* as previously described (26). Strains on the medial surface of the endocortex were calculated from periosteal strains and section properties, based on a scale factor calculated for each genotype and sex as follows,

$$\epsilon_{EM} = \epsilon_{PM} \left(1 - \frac{3}{2} \left(\frac{CT}{Se.Dm} \right) \right) \quad (\text{Eq. 1})$$

where ϵ_{EM} is the peak endocortical strain on the medial surface and CT is the mean thickness of the medial cortex.

Histomorphometry

Both right and left ulnae were fixed in 10% neutral-buffered formalin for 48 h, dehydrated in graded alcohols, cleared in xylene, and embedded in methylmethacrylate. Transverse thick sections (~80 μ m) were cut at the mid-point using a diamond-embedded wire saw (Histosaw; Delaware Diamond Knives, Wilmington, DE). Sections were ground to final thickness of ~20 μ m, and then mounted unstained on standard microscope slides. One section per ulna was viewed at $\times 160$ magnification on a Leitz DMRXE microscope (Leica Mikroskopie und System GmbH, Wetzlar, Germany) and the image captured using a SPOT digital camera (Diagnostic Instruments, Inc., Sterling Heights, MI). The following primary data were collected from the periosteal and endocortical surfaces using Image Pro Plus version 4.1 software (Media Cybernetics, Silver Spring, MD): total perimeter (B.Pm), single label perimeter (sL.Pm), double label perimeter measured along the first label (dL.Pm) and double label area (dL.Ar). From these primary data, the following derived quantities were calculated (27): mineralizing surface (MS/BS = (1/2sL.Pm + dL.Pm)/B.Pm; %), mineral apposition rate (MAR = dL.Ar/dL.Pm/5 days; μ m/day), and bone formation rate (BFR/BS = MAR \times MS/BS \times 3.65; μ m 3 / μ m 2 /year).

In Vivo GFP Monitoring of Load-induced Osteoblast Recruitment

Sixteen to eighteen-week-old Lrp5 $^{++}$, Lrp5 $^{+-}$, and Lrp5 $^{-/-}$ littermates that were also heterozygous for the pOBCol3.6GFP transgene on a mixed CD1/129Sv background, were sedated with isoflurane and given a single bout of ulnar loading (90 cycles; 2 Hz; 1600 μ e). Five Lrp5 $^{++}$ (4 males, 1 female), 7 Lrp5 $^{+-}$ (3 males, 4 females), and 10 Lrp5 $^{-/-}$ (4 males, 6 females) mice were studied. The mice were sacrificed 5 days after the loading bout and the right (loaded) and left (unloaded) ulnae were removed, decalcified, embedded in OCT (Tissue Tek, Elkhart, IN), and sectioned transversely at 6 μ m

thickness using a cryostat (Leica). Sections from the mid-shaft, as judged by the shape of the ulna cross-section, were stained with 4',6-diamidino-2-phenylindole, visualized by fluorescence microscopy, and photographed. A 300–400- μ m arc along the medio-lateral periosteal surface (depending on the size of the bone) was used to determine the total number of periosteal cells and the number of GFP-positive cells. Because Lrp5 $^{+-}$ and Lrp5 $^{++}$ mice had similar periosteal bone growth following mechanical loading, data from these two genotypes were combined and then compared with that from the Lrp5 $^{-/-}$ mice.

Cell Culture Studies

Isolation of Bone Cells—Calvarial osteoblasts were isolated from 3–5 day-old neonatal calvariae from Lrp5 $^{++}$ and Lrp5 $^{-/-}$ mice. Calvariae from the same genotype were grouped and subjected to five sequential 15-min digestions with an enzyme mixture of 1.5 units/ml collagenase P (Roche, Basel, Switzerland) in 0.05% trypsin, 1 mM EDTA on a rocking platform. The first digest was discarded and the second to the fifth digests were passed through a 40- μ m cell strainer (Falcon, BD Biosciences) and pooled. Cells were collected after centrifugation at 2,500 \times g for 8 min and plated in α -modified essential medium with 10% fetal bovine serum, 100 units/ml of penicillin, and 100 μ g/ml of streptomycin in a T25 culture flask (Costar; Corning, Corning, NY) and grown to confluence. After reaching confluence, cells were trypsinized and plated in a T75 culture flask (passage 1). Confluent passage 1 cells were trypsinized and seeded on collagen-coated glass slides for subsequent fluid flow experiment.

Fluid Flow Experiments—Primary cells were seeded at a density of 2,000/cm 2 and grown on 75 \times 38-mm 2 glass slides (Fisher Scientific, Pittsburgh, PA) coated with 10 μ g/cm 2 type I collagen (BD Biosciences). Upon reaching 90% confluence (2–3 days), the cells were serum starved for 24 h in 0.2% fetal bovine serum supplemented culture media (the same media used for flow). During the experiment, fluid flow was applied to the cell monolayer in a parallel plate flow chamber using a closed flow loop (28). This system subjected the cells to a steady laminar flow profile producing a 12 dynes/cm 2 fluid shear stress (FSS). The apparatus was maintained at 37 °C, and the medium was aerated with 95% air, 5% CO $_2$ during the experiment.

Measurement of ATP—Media samples were drawn from the reservoir of the flow loop 1 min after beginning fluid shear stress. An ATP bioluminescence assay containing luciferin/luciferase reagent was used to detect ATP (ATP Bioluminescence Assay kit HS II; Roche) in the media samples. This assay utilizes the conversion of D-luciferin by luciferase into oxyluciferin and light that requires ATP as a co-factor. The resultant luminescence, measured using a Monolight 3010 (BD Biosciences), reflects ATP concentration.

Prostaglandin E₂ (PGE₂) Assay—After 60 min of FSS, the cells were removed from the flow chamber and 2 ml of 0.2% fetal bovine serum media was added onto the monolayer of cells and incubated for 30 min at 37 °C in the incubator. After 30 min, the conditioned media was collected for PGE₂ measurement using a commercially available, competitive binding enzyme immunoassay kit (BioTrak, Amersham Biosciences).

Lrp5 in Bone Anabolic Pathways

TABLE 1

Baseline skeletal phenotype in 18-week-old Lrp5^{+/+}, Lrp5^{+/-}, and Lrp5^{-/-} mice

Values presented are mean \pm S.E.

Parameter	Male				Female			
	Lrp5 ^{+/+} (n = 28–29)	Lrp5 ^{+/-} (n = 27–28)	Lrp5 ^{-/-} (n = 15–29)	Difference, Lrp5 ^{-/-} versus Lrp5 ^{+/+}	Lrp5 ^{+/+} (n = 20)	Lrp5 ^{+/-} (n = 19–20)	Lrp5 ^{-/-} (n = 10–23)	Difference, Lrp5 ^{-/-} versus Lrp5 ^{+/+}
Femoral length (mm)	17.1 \pm 0.1 ^a	16.9 \pm 0.1 ^a	15.9 \pm 0.1 ^b	-7.0%	16.1 \pm 0.2 ^a	16.1 \pm 0.2 ^a	16.0 \pm 0.1	-0.6%
Body mass (g)	28.13 \pm 0.53 ^a	27.59 \pm 0.70 ^a	26.77 \pm 0.61 ^a	-4.8%	21.25 \pm 0.44 ^a	20.74 \pm 0.40 ^a	22.23 \pm 0.59 ^a	4.6%
Midshaft femur geometric properties								
Cortical area (mm ²)	1.13 \pm 0.036 ^a	0.90 \pm 0.030 ^{b,c}	0.76 \pm 0.025 ^b	-32.7%	0.89 \pm 0.020 ^a	0.80 \pm 0.029 ^{c,d}	0.77 \pm 0.024 ^b	-13.5%
Polar moment of inertia (mm ⁴)	0.52 \pm 0.029 ^a	0.32 \pm 0.022 ^{a,b}	0.24 \pm 0.015 ^b	-53.8%	0.32 \pm 0.013 ^a	0.25 \pm 0.017 ^{a,d}	0.24 \pm 0.014 ^b	-25.0%
Distal femur cancellous bone structural properties								
BV/TV (%)	15.0 \pm 1.5 ^a	4.8 \pm 0.6 ^{b,c}	2.9 \pm 0.6 ^{b,c}	-80.7%	10.8 \pm 1.1 ^a	7.5 \pm 1.2 ^{c,d}	6.1 \pm 0.3 ^{b,c}	-43.5%
Tb.N (1/mm)	5.54 \pm 0.24 ^a	3.65 \pm 0.13 ^{a,b}	2.65 \pm 0.14 ^{a,b}	-52.2%	4.65 \pm 0.21 ^a	4.43 \pm 0.29 ^a	4.19 \pm 0.08 ^a	-9.9%
Tb.Th (μ m)	50.6 \pm 1.5 ^a	43.3 \pm 1.7 ^b	40.5 \pm 2.8 ^b	-20.0%	45.3 \pm 1.0 ^c	40.5 \pm 1.5 ^d	39.7 \pm 1.1 ^d	-12.4%
Tb.Sp (μ m)	189.7 \pm 7.0	282.9 \pm 9.9 ^{b,c}	396.8 \pm 23.9 ^{a,b}	109.2%	220.8 \pm 8.8	238.1 \pm 13.4 ^c	244.0 \pm 5.5 ^{a,d}	10.5%
Connectivity density (mm ⁻³)	155.8 \pm 20.6	25.7 \pm 4.7 ^{a,b}	17.5 \pm 5.0 ^{b,c}	-88.8%	132.9 \pm 14.3	88.8 \pm 15.6 ^{a,d}	52.6 \pm 7.4 ^{b,c}	-60.4%
SMI	2.55 \pm 0.15	3.61 \pm 0.08 ^{a,b}	3.51 \pm 0.21 ^b	37.6%	2.60 \pm 0.10	3.01 \pm 0.09 ^{a,d}	3.21 \pm 0.07 ^b	23.5%
Vertebral cancellous bone structural properties (L5)								
BV/TV (%)	27.0 \pm 1.2	18.5 \pm 0.4 ^{a,b}	15.3 \pm 0.8 ^{a,b}	-43.3%	26.5 \pm 1.0	24.2 \pm 1.4 ^a	23.7 \pm 0.9 ^{a,d}	-10.6%
Tb.N (1/mm)	6.0 \pm 0.20 ^a	4.61 \pm 0.11 ^b	4.13 \pm 0.12 ^b	-31.2%	5.03 \pm 0.22 ^a	4.57 \pm 0.25	4.50 \pm 0.07 ^d	-10.5%
Tb.Th (μ m)	58.4 \pm 1.6	54.4 \pm 1.3 ^d	48.9 \pm 1.6 ^b	-16.3%	58.8 \pm 1.1	57.6 \pm 1.0	53.9 \pm 0.9 ^{a,b}	-8.3%
Tb.Sp (μ m)	182.1 \pm 6.4 ^a	231.7 \pm 6.2 ^b	258.8 \pm 9.3 ^b	42.1%	221.9 \pm 8.3 ^a	244.2 \pm 11.2 ^d	252.0 \pm 4.8 ^b	13.6%
Connectivity density (mm ⁻³)	263.8 \pm 15.9 ^c	155.8 \pm 8.1 ^b	150.5 \pm 9.0 ^{a,b}	-42.9%	208.5 \pm 25.9 ^c	181.3 \pm 20.6	235.1 \pm 11.8 ^a	12.8%
SMI	1.04 \pm 0.12 ^a	1.70 \pm 0.05 ^{a,b}	1.77 \pm 0.10 ^{a,b}	70.2%	0.51 \pm 0.14 ^a	0.65 \pm 0.15 ^a	0.65 \pm 0.14 ^a	27.5%
Midshaft femur mechanical properties								
Ultimate force (N)	24.9 \pm 1.1 ^a	18.4 \pm 0.3 ^{a,b}	14.0 \pm 0.2 ^{b,c}	-43.8%	20.3 \pm 0.5 ^a	16.1 \pm 0.7 ^{a,b}	15.7 \pm 0.3 ^{b,c}	-22.7%
Stiffness (N/mm)	106.7 \pm 3.7 ^a	81.0 \pm 2.5 ^b	60.9 \pm 1.4 ^{a,b}	-42.9%	93.2 \pm 2.1 ^a	76.3 \pm 3.0 ^b	72.9 \pm 3.3 ^{a,b}	-21.8%
Work to failure (mJ)	6.28 \pm 0.5	4.97 \pm 0.4 ^d	4.05 \pm 0.39 ^b	-35.5%	6.27 \pm 0.46	5.12 \pm 0.31 ^d	4.18 \pm 0.29 ^b	-33.3%
Vertebral mechanical properties (L5)								
Ultimate force (N)	37.9 \pm 1.5	27.6 \pm 0.5 ^b	18.6 \pm 1.2 ^{b,c}	-50.9%	35.4 \pm 2.5	30.9 \pm 3.7	25.2 \pm 2.2 ^{b,c}	-28.8%
Stiffness (N/mm)	169.9 \pm 8.7	137.1 \pm 8.1 ^d	112.6 \pm 7.9 ^b	-33.7%	159.5 \pm 18.0	153.7 \pm 17.9	134.4 \pm 12.7	-15.7%
Work to failure (mJ)	16.7 \pm 1.0	11.6 \pm 0.7 ^b	9.15 \pm 0.65 ^{b,c}	-45.2%	17.4 \pm 1.2	14.0 \pm 1.8 ^d	12.5 \pm 0.9 ^{b,c}	-28.2%

^ap < 0.01, significantly different between sexes for a given genotype.

^bp < 0.01, significantly different from the WT controls.

^cp < 0.05, significantly different between sexes for a given genotype.

^dp < 0.05, significantly different from the WT controls.

PGE₂ release into the conditioned media was normalized to total cell protein. The protein assay was accomplished by the Amido Black method (29).

Western Blotting—Cells were washed with cold phosphate-buffered saline (1 time), lysed with two times SDS sample buffer (5 mM HEPES, pH 7.9, 150 mM NaCl, 26% glycerol, 1.5 mM MgCl₂, 0.2 mM EDTA, 0.5 mM dithiothreitol, and 0.5 mM phenylmethylsulfonyl fluoride) on ice and immediately boiled for 5 min. The protein samples were centrifuged at 14,000 \times g for 10 min at room temperature and the supernatant was retained and electrophoresed on a 10% SDS-polyacrylamide gel at 20 μ g of protein per lane. The proteins were electrotransferred to a nitrocellulose membrane and blocked in Tris-buffered saline containing 5% nonfat dry milk and 0.1% Tween 20 (TBST). After blocking, the membranes were incubated with an anti-osteopontin antibody (1:100, AssayDesigns, Inc., Ann Arbor, MI), anti-vinculin antibody (1:500, Sigma), or anti-extracellular signal-regulated kinase (ERK) 1/2 antibody (1:500; Cell Signaling, Inc., Danvers, MA) and anti-phospho-ERK1/2 antibody (1:500; Cell Signaling, Inc.) overnight at 4 °C. The membranes were washed 3 times in TBST, incubated with appropriate horseradish peroxidase-conjugated secondary antibodies, washed an additional 3 times in TBST, and developed using the enhanced chemiluminescence (ECL) method.

Statistical Analysis—Data with multiple time points, such as BMC/body weight were first compared by repeated anal-

ysis of variance measures. When analysis detected significant differences between genotypes, then significance at each time point was assessed by Tukey-Kramer post hoc test. Other phenotype values among genotype for a given sex were compared by one-way analysis of variance. Gender comparisons were performed using a two-way analysis of variance with sex and genotype as independent variables. Periosteal dose responses to different mechanical strains within genotypes were tested for significance with least-squares regression. Differences in slope and x intercept (bone formation versus mechanical strain) among genotypes were tested for significance by analysis of covariance. When analysis of covariance detected significant differences among slopes, Tukey's HSD tests were performed to test pairwise comparisons of slopes and x intercepts (osteogenic threshold). Strains on the endocortical surface were much lower than periosteal strains; consequently, a large portion of the loaded bones were below the osteogenic threshold and exhibited no osteogenic response to loading. Therefore, the endocortical dose response was analyzed using the segmented regression model PROC NLIN in Jmp version 4 (SAS Institute Inc., Cary, NC) in which a quadratic equation was fit to each data series. Break points (x_0), where the segments join, were solved iteratively according to the routine $y = a + bx + cx^2$, if $x < x_0$, and $y = p$ if $x > x_0$ until the correlation was maximal (30). The numbers of periosteal cell nuclei and GFP+ periosteal cells in loaded versus unloaded limbs, and in Lrp5^{+/+}/

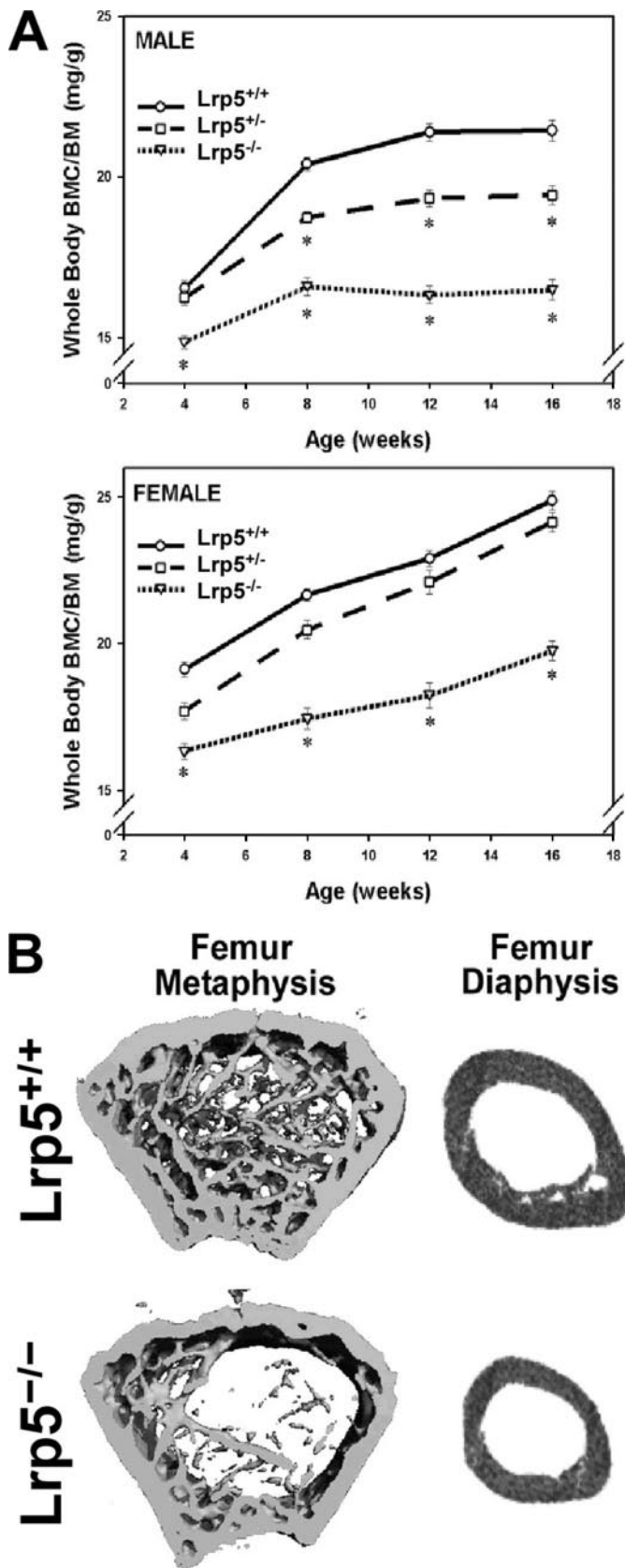


FIGURE 2. Skeletal consequences of Lrp5 deficiency. *A*, bone mineral content acquisition curves in Lrp5^{-/-} and Lrp5^{+/+} mice measured at 4-week intervals, beginning at 4 weeks of age. Whole body bone mineral content per unit body mass (BMC/BM) was significantly lower in both male and female Lrp5^{-/-} mice, compared with Lrp5^{+/+} mice, at all time points examined

Lrp5^{+/-} and Lrp5^{-/-} mice, were compared using Student's *t* test. For all tests, statistical significance was set at $\alpha = 0.05$.

RESULTS

Lrp5-null Mice Exhibit Deficient Bone Mass, Geometry, Structure, and Strength, despite Normal Body Weight and Limb Length—To begin assessing the role of Lrp5 in the skeletal phenotype, we collected animal weights, measured femur lengths, and assessed bone mineral content using pDEXA in wild-type (Lrp5^{+/+}), heterozygous (Lrp5^{+/-}), and Lrp5-null (Lrp5^{-/-}) mice. Within both sexes, the average body weight was statistically similar among Lrp5^{+/+}, Lrp5^{+/-}, and Lrp5^{-/-} mice (Table 1). Femur lengths were similar in female Lrp5^{+/+}, Lrp5^{+/-}, and Lrp5^{-/-} mice, but male Lrp5^{-/-} mice exhibited significantly shorter femora at 18 weeks of age (Table 1). However, consistent with a previous study (10), we observed that Lrp5^{-/-} mice have a low bone mass phenotype. The difference in total body BMC per unit body mass (BMC/BM) between Lrp5^{-/-} and Lrp5^{+/+} mice became significant at 4 weeks of age and persisted through adulthood, reaching a 23% deficit by 16 weeks of age in both male and female Lrp5^{-/-} mice (Fig. 2*A*). Interestingly, male Lrp5^{+/-} mice had significantly less bone mass than Lrp5^{+/+} controls, but this was not the case for the female Lrp5^{+/-} mice.

μ CT analysis in adult mice revealed that the midshaft femur cross-sectional area and the polar moment of inertia (an estimate of the ability of the structure to resist torsional loading (31)) were significantly lower (by 25–50%) in Lrp5^{-/-} mice compared with Lrp5^{+/+} controls (Table 1). Genotype-related disparities were also detected in the trabecular envelope of the distal femur and spine (Fig. 2*B*). For example, BV/TV was 81% lower in male Lrp5^{-/-} femora than in their Lrp5^{+/+} controls. The Lrp5 deficiency appeared to have a greater impact in male mice compared with females, and the skeletal effects were greater at the distal femur compared with spine. Other measures of cancellous architecture followed similar trends to those reported above for BV/TV, with the exception of trabecular spacing (Tb.Sp), which, as expected, increased significantly in Lrp5^{-/-} mice.

To further characterize the skeletal phenotype associated with Lrp5 deficiency, we dissected out whole femora, and 5th lumbar vertebrae from 16-week-old Lrp5^{+/+}, Lrp5^{+/-}, and Lrp5^{-/-} mice, and subjected them to biomechanical testing. The disparities observed in bone mass among the Lrp5^{+/+}, Lrp5^{+/-}, and Lrp5^{-/-} mice were reflected in their biomechanical properties. Under 3-point bending conditions, the femoral shafts from Lrp5^{-/-} were significantly more compliant, absorbed significantly less energy before failing, and failed at a

(4–16 weeks). Heterozygous males but not females exhibited a statistically significant intermediate phenotype. *B*, micro-CT reconstructions of femoral metaphyses and diaphyses from 18-week-old male Lrp5^{-/-} and Lrp5^{+/+} mice. Trabecular and cortical bone envelopes were adversely affected by the loss of Lrp5 signaling. The femoral metaphysis images are reconstructions from 60 to 100 individual μ CT slices. The femoral diaphysis images are individual μ CT slices through the midshaft. Note the obvious deficiency in trabecular bone volume and femoral shaft size in the Lrp5^{-/-} mice. Results were similar in female mice.

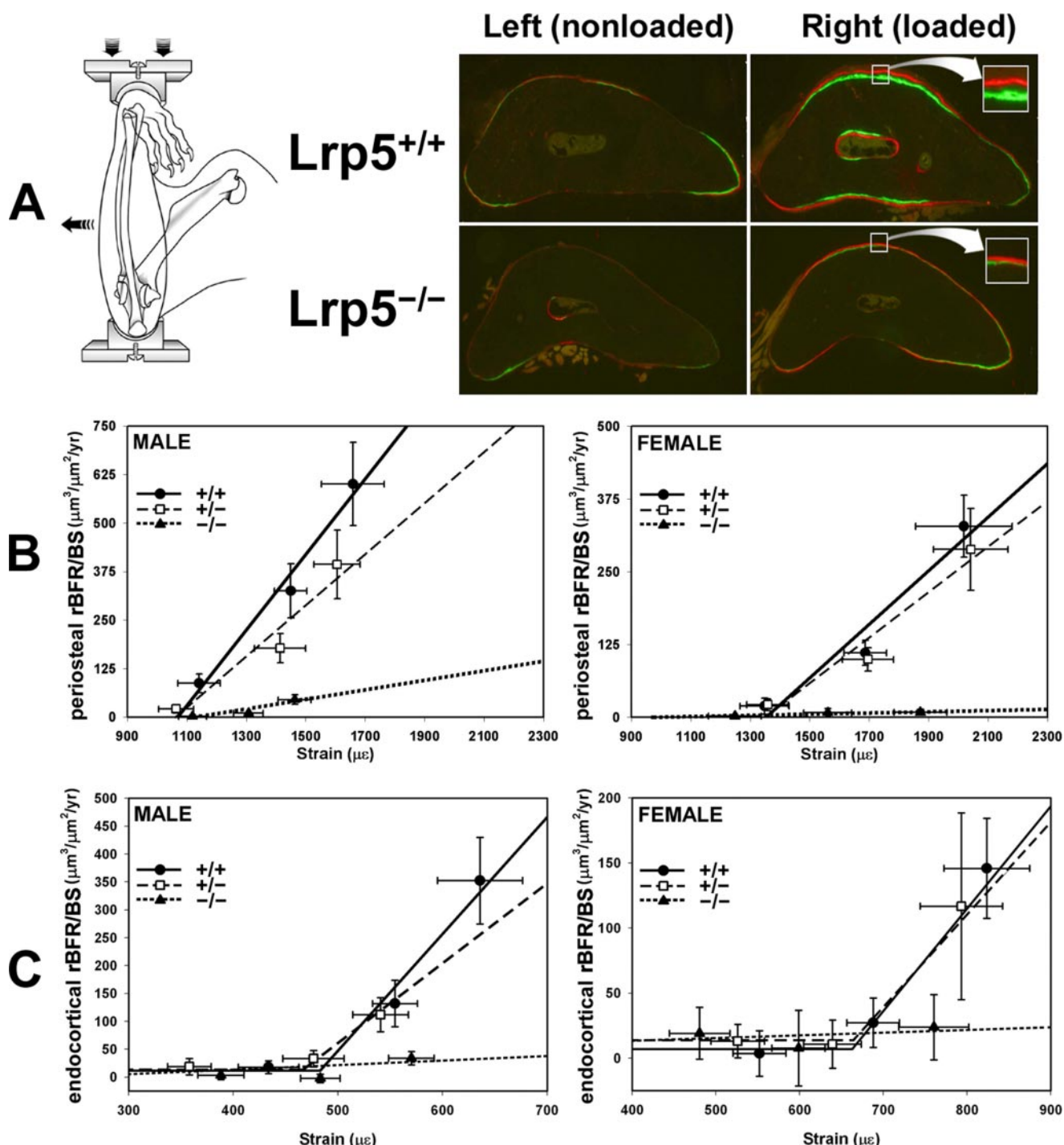


FIGURE 3. *Lrp5^{-/-}* mice have impaired osteogenic responses to mechanical loading. **A**, diagram of the noninvasive mouse ulna loading model, which applies cyclic compression to the forearm to produce mediolateral bending (due to natural curvature of the ulna) to mechanically stimulate ulnar bone tissue in adult mice *in vivo*. Midshaft ulnar tissue sections from control and loaded forearms among male *Lrp5^{+/+}* and *Lrp5^{-/-}* mice given fluorochrome injections after loading show a robust bone formation response on the medial (*inset*) and lateral surfaces of the loaded *Lrp5^{+/+}* ulna, yet almost no response can be observed in the loaded *Lrp5^{-/-}* ulna. **B**, graphs depicting relative bone formation rates (rBFR/BS) on the periosteal surface of the midshaft ulna in response to applied mechanical strain in all 3 genotypes and both sexes. *Lrp5^{-/-}* mice were severely impaired in their ability to respond anabolically to normal tissue strains (88% reduction in males and 99% reduction in females). **C**, graphs depicting endocortical rBFR/BS in response to applied mechanical strain in all 3 genotypes and both sexes. *Lrp5^{+/+}* and *Lrp5^{+/-}* mice demonstrate a dose-response relation, which is absent (not significantly different from zero) in *Lrp5^{-/-}* mice.

significantly lower force than *Lrp5^{+/+}* control femora (Table 1). The difference between *Lrp5^{+/+}* and *Lrp5^{-/-}* properties ranged from 30 to 36% for all of the parameters examined. The *Lrp5^{+/-}* femora exhibited an intermediate phenotype, but the difference between *Lrp5^{+/+}* and *Lrp5^{+/-}* mechanical proper-

ties was significant only for ultimate force. Vertebral compressive strength (F_U) was reduced in male and female *Lrp5^{-/-}* mice by 51 and 29%, respectively (Table 1). As in the femur, vertebral stiffness and work to failure followed similar trends as F_U .

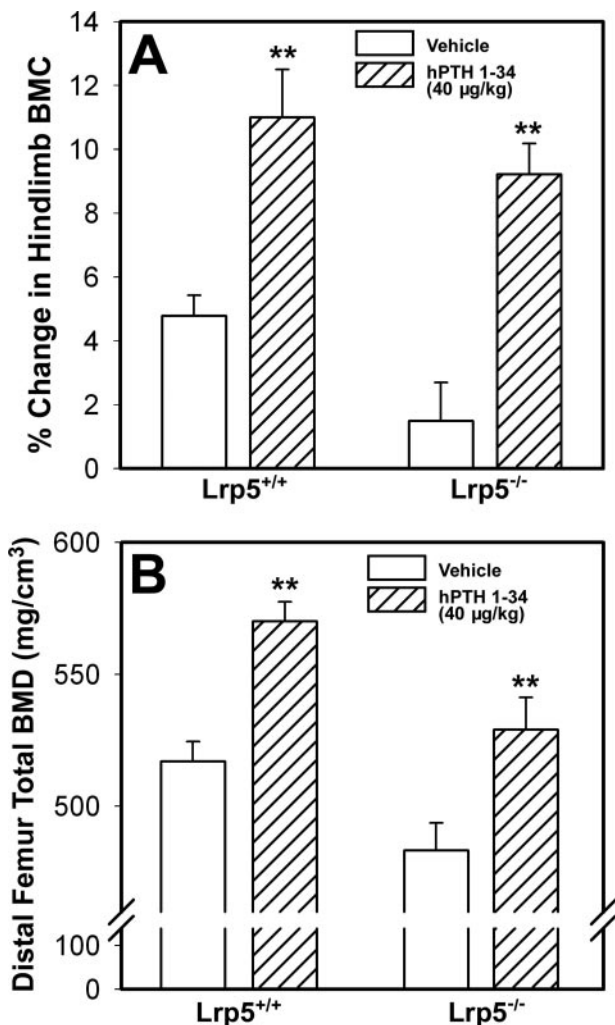


FIGURE 4. Four weeks of intermittent PTH treatment (40 µg/kg/day) causes similar increases in bone mass in Lrp5^{-/-} and Lrp5^{+/+} mice. *A*, graph depicting increased hindlimb bone mineral content (measured longitudinally via *in vivo* pixiMUS scans). Male and female animals were pooled because no significant sex effects were detected. Note that the percent change in hindlimb BMC compared with vehicle treated mice was not significantly different between Lrp5^{-/-} and Lrp5^{+/+} mice. Double asterisks indicate significant differences from vehicle treated animals. *B*, graph depicting increased volumetric BMD at the distal femur (measured with pQCT). Data from males are shown; females showed similar trends. Note that the percent change in distal femur total BMD compared with vehicle treated mice was not significantly different between Lrp5^{-/-} and Lrp5^{+/+} mice. Double asterisks indicate significant differences from vehicle treated animals.

Lrp5^{-/-} Mice Exhibit Almost No Osteogenic Response to Mechanical Loading *In Vivo*—To directly investigate the role of Lrp5 in bone mechanoresponsiveness *in vivo*, we subjected Lrp5^{+/+}, Lrp5^{+/-}, and Lrp5^{-/-} mice to *in vivo* mechanical loading and measured the bone formation response histomorphometrically. Cross-sections of loaded ulnae from Lrp5^{+/+} mice revealed new periosteal and endocortical lamellar bone formation (bone between fluorochrome labels), mostly on the medial and lateral quadrants (Fig. 3A). In contrast, Lrp5^{-/-} mice ulnae showed very limited double labeling in the loaded ulnae. The suppression of load-induced bone formation was evident in both male and female Lrp5^{-/-} mice, but females exhibited the most dramatic lack of response. The relative periosteal bone formation rate (BFR/BS in the loaded ulna minus

BFR/BS in the nonloaded ulna) was roughly 99% lower in female Lrp5^{-/-} mice compared with female Lrp5^{+/+} mice (Fig. 3B). The heterozygous mice responded to a lesser extent than Lrp5^{+/+} animals, but statistical difference from Lrp5^{+/+} was reached only for the males. The endocortical surface showed similar trends as the periosteal surface. Lrp5^{-/-} mice failed to exhibit a bone formation response on the endocortical surface, as revealed by a strain *versus* rBFR/BS regression that was not significantly different from zero (Fig. 3C).

Parathyroid Hormone Is Equally Anabolic in the Lrp5^{-/-} and Lrp5^{+/+} Mouse Skeleton—To assess the requirement of Lrp5 receptor signaling in response to a well established bone anabolic agent, we treated 12-week-old mice for 4 weeks with daily injections of PTH-(1–34) (40 µg/kg) or vehicle, and monitored whole body and hindlimb bone mass changes by baseline (day 0) and final (day 28) pDEXA scans, and by femoral pQCT scans at sacrifice. Percent change in bone mineral content (baseline BMC *versus* final BMC for each animal) showed no significant sex effect, so male and female data were pooled. PTH improved whole body BMC by 10.7% in Lrp5^{-/-} mice and 7.2% in Lrp5^{+/+} mice. Analysis of variance revealed significant overall genotype and treatment effects ($p < 0.05$), but a significant interaction between genotype and treatment was not detected, suggesting that PTH enhanced hindlimb BMC significantly and equally in Lrp5^{-/-} and Lrp5^{+/+} mice (Fig. 4A).

pQCT measurements of the mineral content in the distal femur revealed significant sex effects; consequently, male and female data were treated separately. Among males, 4 weeks of PTH treatment increased distal femur total BMD by 10.2 and 9.5% in Lrp5^{+/+} and Lrp5^{-/-} mice, respectively (Fig. 4B). Among females, 4 weeks of PTH treatment increased distal femur total BMD by 12.2 and 9.0% in Lrp5^{+/+} and Lrp5^{-/-} mice, respectively. Whereas the PTH-induced increase in BMD was significant for both sexes and genotypes, the degree of enhancement was not statistically different between genotypes of the same sex.

Osteoblast Recruitment to Mechanically Loaded Bone Surfaces Is Normal in Lrp5^{-/-} Mice—After discovering a nearly complete absence of the osteogenic response to mechanical loading in Lrp5^{-/-} mice, we sought to understand whether the deficit was related to inadequate recruitment/activation of osteoblasts at bone surfaces after mechanical loading. To this end, we bred the Lrp5^{-/-} alleles onto the pOCBCol3.6GFP mouse strain, which expresses GFP in early osteoblasts. Normally, osteoblasts begin to appear at strained surfaces 3–5 days after a mechanical loading bout (32, 33). We sacrificed Lrp5^{-/-} pOCBCol3.6GFP, Lrp5^{+/-} pOCBCol3.6GFP, and Lrp5^{+/+} pOCBCol3.6GFP mice 5 days after a single ulnar loading session, and counted the total number of cells and the number of GFP+ cells on the lateral ulnar periosteum.

We observed a difference in the number of GFP+ cells, but not in the total number of periosteal cells in the loaded *versus* non-loaded ulnae of all genotypes (Fig. 5). This result suggests that at 5 days following the ulnar stimulation with mechanical load, the periosteum had responded to mechanical stimulation by activating cells already at the periosteal surface, and not by recruiting new cells or stimulating periosteal cell division.

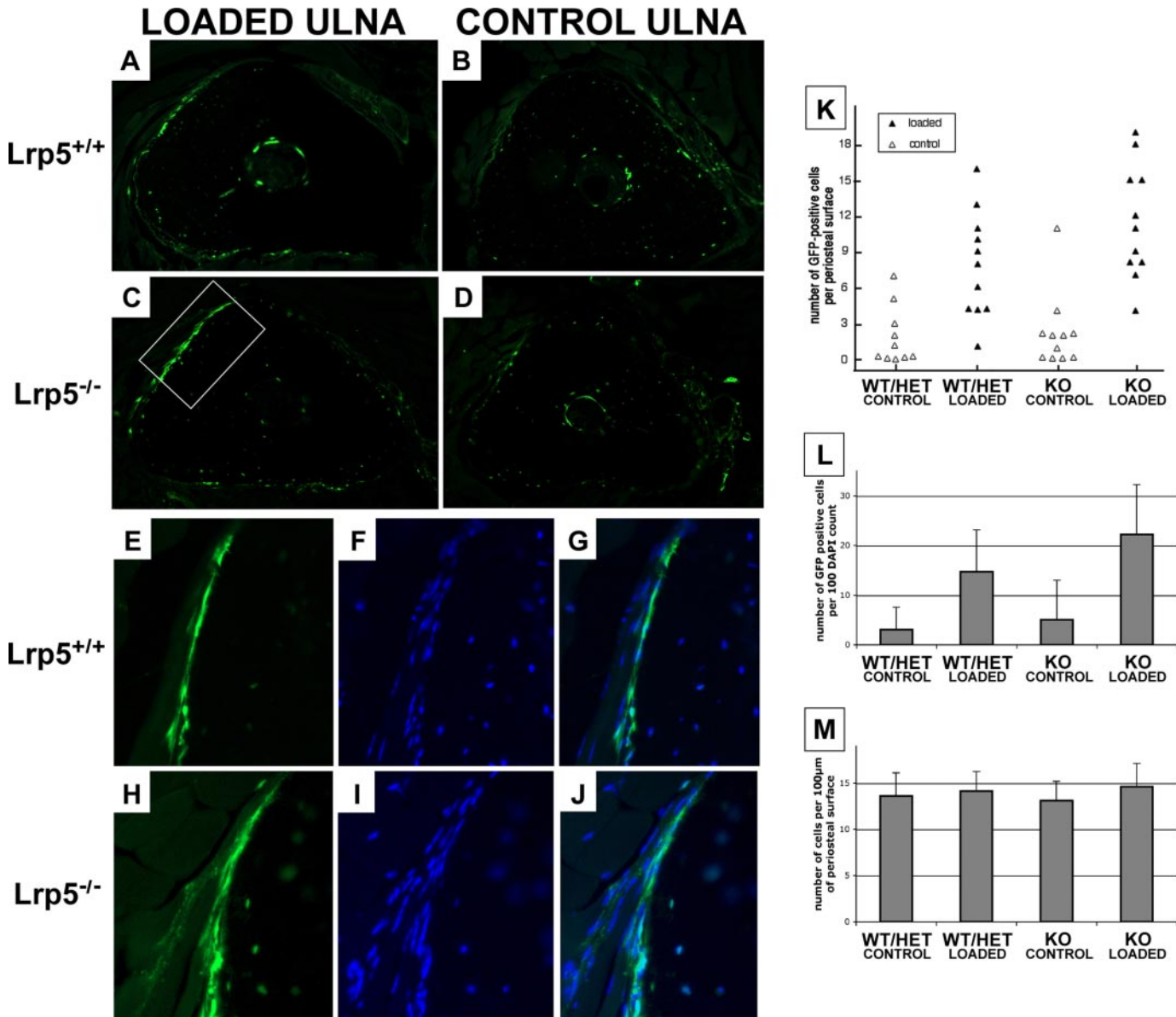


FIGURE 5. The initial recruitment/reactivation of periosteal cells following mechanical loading is preserved in Lrp5^{-/-} mice. *A–D*, photomicrographs of representative cross-sections through the midshaft of the ulna from an Lrp5^{+/+} and an Lrp5^{-/-} mouse following a single bout of mechanical loading. The periosteal surfaces of the unloaded ulnae from Lrp5^{+/+} (*B*) and Lrp5^{-/-} (*D*) mice appear quiescent because very few of the periosteal cells are GFP+. In contrast, GFP-expressing cells were observed along the periosteal surfaces of the loaded ulnae from the Lrp5^{+/+} (*A*) and Lrp5^{-/-} (*C*) mice, indicating that loading led to either the recruitment or activation of osteoblast precursor cells. *E–J*, photomicrographs of the region along the periosteal surface (white box indicated in panel *C*) that consistently demonstrated increased GFP expression in loaded versus unloaded ulnae. This region was used to determine the total number of periosteal cells and the fraction of periosteal cells that were GFP positive in Lrp5^{+/+} (*E–G*) and Lrp5^{-/-} (*H–J*) mice. Counted cells were only those at the periosteal surface, and not from embedded osteocytes or from adjacent tenocytes or myocytes. Analysis of pooled male and female mouse ulnar sections revealed no significant differences between the total number of cells per 100 μ m of periosteal arc, between loaded and unloaded limbs, or between Lrp5^{-/-} and Lrp5^{+/+}/Lrp5^{+/+} mice (*M*), indicating that the loading most likely activates existing cells rather than recruit new cells. Although there was a significant increase in the frequency of GFP-positive cells in the loaded limbs versus the unloaded limbs (*K*), there was no difference between the loaded limbs from Lrp5^{+/+}/Lrp5^{+/+} versus Lrp5^{-/-} mice (*L*).

Despite loaded ulnae having significantly more GFP+ cells than non-loaded ulnae, there were no differences between Lrp5^{-/-} and Lrp5^{+/+}/Lrp5^{+/+} mice (Fig. 5). This suggests that the absence of Lrp5 function does not affect the early stages of the osteogenic response to mechanical stimulation.

Primary Osteoblasts from Lrp5^{-/-} Mice Do Not Exhibit Deficiencies in Early Mechanotransduction Signaling in Vitro, but Later Stage Markers Are Affected—To further study the role of Lrp5 in osteoblast mechanotransduction, we cultured primary osteoblasts from Lrp5^{+/+} and Lrp5^{-/-} neonatal mouse cal-

variae, subcultured them onto collagen-coated glass slides, and subjected them to fluid shear stress (12 dyne/cm²) to simulate mechanical loading *in vitro* (Fig. 6*A*). As has been shown by others (34, 35), FSS induces osteoblasts to release ATP into the culture media after 1 min. Primary osteoblasts cultured from Lrp5^{+/+} and Lrp5^{-/-} mice released ATP in response to FSS, and Lrp5^{-/-} cells were actually more responsive than Lrp5^{+/+} cells (Fig. 6*B*). We also measured PGE₂, an important mediator of mechanical loading in osteoblasts (36–38). Sixty minutes of FSS induced a significant release of PGE₂ into the culture media

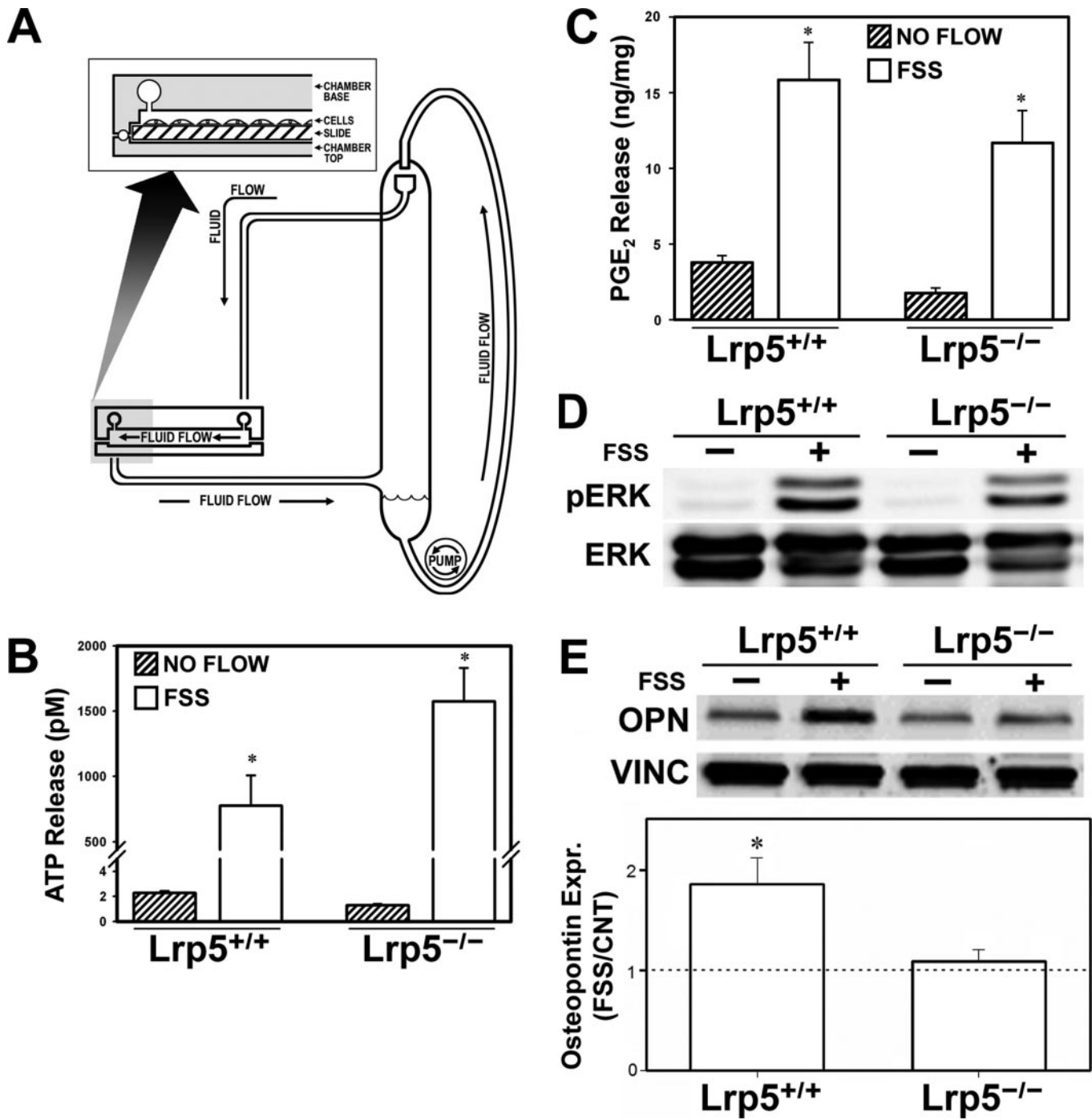


FIGURE 6. Lrp5^{-/-} and Lrp5^{+/+} primary calvarial osteoblasts have a similar early response to fluid shear stress, but a different late response. **A**, schematic depicting fluid flow device for applying shear stress to primary osteoblasts. Fluid is pumped to an upper reservoir, which creates a hydrostatic pressure head and drives fluid across the surface of cells mounted into a parallel plate flow chamber below (*inset*). **B**, graph depicting the release of ATP into the media of primary calvarial osteoblasts cultured from Lrp5^{+/+} and Lrp5^{-/-} mice after 1 min of FSS. Note that Lrp5^{+/+} and Lrp5^{-/-} cells release ATP in response to FSS and (asterisks indicate significant differences from no flow treated cells) that Lrp5^{-/-} osteoblasts release more ATP than do Lrp5^{+/+} osteoblasts ($p < 0.05$). **C**, graph depicting the release of PGE₂ into the media of primary calvarial osteoblasts cultured from Lrp5^{+/+} and Lrp5^{-/-} mice after 1 h of FSS. Note that Lrp5^{+/+} and Lrp5^{-/-} cells release PGE₂ in response to FSS (asterisks indicate significant differences from no flow treated cells). **D**, Western blots of protein extracts from Lrp5^{+/+} and Lrp5^{-/-} osteoblasts lysed after 30 min of FSS, separated by SDS-PAGE, and immunodetected with phospho-ERK (*upper panel*) and total ERK (*lower panel*) specific antibodies. Note that Lrp5^{+/+} and Lrp5^{-/-} osteoblasts are able to phosphorylate ERK in response to FSS. **E**, Western blots of protein extracts from Lrp5^{+/+} and Lrp5^{-/-} osteoblasts lysed after 8 h of FSS, separated by SDS-PAGE, and immunodetected with anti-osteopontin (OPN) (*upper panel*) and anti-vinculin (VINC, which serves as a loading control) (*lower panel*) specific antibodies. Note that osteopontin protein expression was enhanced in Lrp5^{+/+} but not in Lrp5^{-/-} cells, indicating that later stages of mechanoresponsiveness are affected by the loss of Lrp5 signaling.

(4.5–6-fold over static culture cells) in both Lrp5^{+/+} and Lrp5^{-/-} cells, but no genotype difference in FSS-induced PGE₂ release was detected (Fig. 6C). Next, we investigated the ability

of fluid shear stress to activate the mitogen-activated protein kinase (MAPK) cascade in Lrp5^{+/+} and Lrp5^{-/-} cells, because MAPK signaling is essential for the expression of several genes

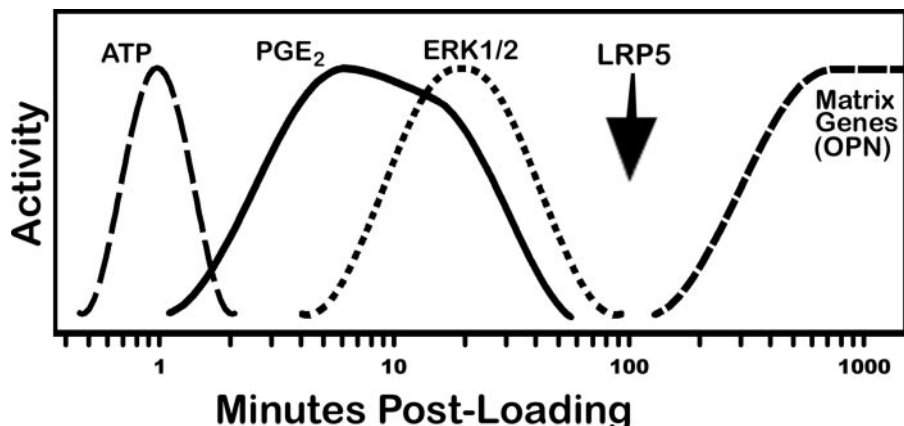


FIGURE 7. Graphical representation of major mechanotransduction signaling events, with a putative sequence for Lrp5 signaling. Within 1 min of loading, bone cells release a bolus of ATP (34) followed by PGE₂ release (65), and MAPK signaling (ERK1/2 activation) (40), ultimately resulting in the expression of bone matrix genes, including osteopontin and collagen (40). Our data suggest that Lrp5 signaling is downstream of the MAPK cascade but upstream of osteopontin and other matrix genes.

linked to mechanotransduction (39, 40). In both Lrp5^{+/+} and Lrp5^{-/-} osteoblasts, 30 min of shear stress induced significant ERK1/2 activation, compared with genotype-matched static cells not subjected to flow (Fig. 6D). No difference in shear-induced ERK1/2 activation was detected between Lrp5^{+/+} and Lrp5^{-/-} cells. Thus, MAPK signaling appears intact in Lrp5-deficient cells.

Because we observed no deficiencies in Lrp5^{-/-} osteoblasts with respect to early cellular responses to FSS, we looked to a later marker of mechanotransduction. Osteopontin expression has been shown to correlate with mechanically induced bone formation *in vivo* (41, 42) and is up-regulated by fluid shear stress *in vitro* (40, 43–45). Eight hours after initiation of fluid shear stress of Lrp5^{+/+} and Lrp5^{-/-} osteoblasts, we measured osteopontin protein expression by Western blotting. Osteopontin production was significantly enhanced in Lrp5^{+/+} but not Lrp5^{-/-} cells (Fig. 7B). These data suggest that the later responses to mechanical stimulation, such as matrix protein production, are impaired by the loss of Lrp5 signaling.

DISCUSSION

The main objective of our study was to understand the role of Lrp5 in the skeletal response to mechanical loading. Lrp5 null mice clearly demonstrate that Lrp5 has an important role in normal bone acquisition during growth and development. Loss of Lrp5 signaling results in a smaller, structurally inferior skeleton that is severely compromised in its ability to respond to mechanical stimuli, but responds normally to intermittent PTH treatment. Thus, our data suggest that one of the main mechanisms through which Lrp5 signaling exerts its effects on the skeleton is in responding to mechanical signals.

The results from our PTH experiments, indicating that intermittent PTH treatment was fully anabolic in Lrp5^{-/-} mice, were surprising. We had anticipated that Lrp5 inactivation would inhibit the anabolic response to PTH based on a report in the literature (46). Most data support an integral role for LRP5 in the “canonical” Wnt signaling pathway, where activation by a family of secreted glycoproteins, Wnts, at the cell surfaceulti-

mately leads to the nuclear accumulation of β -catenin. Nuclear β -catenin complexes with members of the T cell factor/LEF transcription factor family to regulate gene transcription. *In vitro*, UMR-106 cells treated with PTH exhibit an accumulation of β -catenin and enhanced T cell factor-mediated transcription activity, two hallmarks of canonical Wnt signaling. Furthermore, continuous PTH exposure was reported to suppress Dkk1 expression in the rat femur, which in turn should increase signaling through Lrp5 (46).

Our findings could have resulted from PTH utilizing the canonical Wnt signaling cascade by acting

through the closely related receptor Lrp6, which is not altered in the Lrp5-null mice. Like Lrp5, Lrp6 has been shown to influence bone mass in mice (47) and Lrp5 and Lrp6 have overlapping patterns of expression, including in skeletal tissues, and are both inhibited by Dkk1. However, intermittent PTH treatment has been shown to increase bone formation in mice over-expressing Dkk1, which argues against PTH action requiring functioning Lrp5 or Lrp6 receptors (48). Furthermore, PTH is known to affect other signaling pathways, such as insulin-like growth factor I receptor signaling (49). Our finding that PTH can promote bone anabolism in Lrp5 mutant mice has been independently supported by a study (published in abstract form, Ref. 11) that found that 6 weeks of intermittent PTH treatment (80 μ g/kg/d) increased osteoblast surface and femoral cortical thickness in Lrp5^{-/-} mice to the same degree as in wild-type mice. Because the anabolic effects of intermittent PTH do not require a functioning Lrp5 receptor in mice, it is possible that intermittent PTH therapy in patients with OPPG or in heterozygous LRP5 mutation carriers may help increase bone mass and prevent fractures. Lrp5 mutant mice that were given a daily dose of lithium chloride also exhibited an increase in bone mass (20). LiCl is postulated to bypass the Lrp5 deficiency by activating canonical Wnt signaling downstream of the Wnt-Lrp5-Frizzled receptor complex. Our studies do not preclude PTH exerting similar anabolic effects by modulating canonical Wnt signaling downstream of the Wnt-Lrp5-Frizzled receptor complex.

In contrast to PTH responsiveness, skeletal mechanoresponsiveness was severely suppressed in the Lrp5^{-/-} mice. The reproducible bone formation response that is elicited by *in vivo* ulnar loading was nearly lost in Lrp5-null mice. This was especially true for female mice, which exhibited a ~99% reduction in relative periosteal bone formation rate compared with Lrp5^{+/+} controls. Our data complement mechanotransduction studies conducted in the high bone mass mutation transgenic mice. Mice expressing a transgene for the high bone mass mutation in Lrp5 (G171V) exhibit a greater osteogenic response to mechanical loading *in vivo* than normal, non-trans-

genic mice (50). Interestingly, the G171V mutant mouse lost less bone than wild-type in response to disuse, but the bone loss occurring from a nonmechanical challenge (ovariectomy) was the same in G171V and wild-type mice. Collectively, these observations highlight the key role of Lrp5 signaling in skeletal mechanotransduction.

Interestingly, Lrp5^{-/-} mice do not appear to have a deficiency in recruiting/activating osteoblasts to the ulnar surface after a loading bout. Normally, after a mechanical loading session, osteoblasts appear at bone surfaces subjected to high mechanical strains 3–5 days after loading, and then begin synthesizing matrix that will ultimately become mineralized (32, 33). A deficiency in osteoblast recruitment/activation at loaded surfaces is one potential mechanism by which impaired mechanotransduction can be manifest. However, use of the pOBCol3.6GFP mouse allowed us to track the load-induced osteoblast appearance in the otherwise quiescent ulnar periosteal surface. In tissue sections taken from these mice, we found equal numbers of periosteal cell nuclei in loaded and unloaded ulnas, suggesting that the appearance of osteoblasts 5 days after loading represents activation of previously quiescent cells, rather than cell division or recruitment of new cells. Importantly, Lrp5^{-/-} and wild-type mice had comparable increases in the numbers of GFP+ early osteoblasts at the periosteal surface following mechanical loading. These data indicate that the Lrp5^{-/-} osteoblasts are able to be activated by mechanical loading and imply that the defective periosteal bone apposition response caused by Lrp5 deficiency is in the further maturation of these osteoblasts. This conjecture is supported by *ex vivo* studies in which we compared the responsiveness of Lrp5^{-/-} and Lrp5^{+/+} primary osteoblasts to fluid shear stress. Lrp5 deficiency has little effect on early mediators of mechanical signaling, such as ATP and PGE₂ release or ERK1/2 activation, which is detectable within seconds or minutes of mechanical stimulation. However, Lrp5^{-/-} osteoblasts responded differently than Lrp5^{+/+} cells with respect to up-regulation of osteopontin expression, which normally occurs 8 to 24 h after a mechanical stimulus (43–45, 51–53). Some early mediators of mechanical signaling, such as prostacyclin (54) and nitric oxide (55), were not measured so we cannot be certain that all early mediators are unaffected by Lrp5 deficiency.

Mechanical loading (*e.g.* exercise) is an effective means to increase bone mass, prevent bone loss, and perhaps most importantly, reduce fracture susceptibility. The exercise-induced increase in bone strength occurs because new bone formation is targeted to skeletal surfaces experiencing large mechanical strains, *i.e.* bone is added where it is most needed. This targeting mechanism allows for the addition of a small amount of bone to confer large increases in mechanical properties of the tissue by creating a more mechanically favorable geometry. For example, increasing bone mineral content of a limb bone by only 5–10% via mechanical loading is associated with a 65% improvement in ultimate force, a 90% improvement in fracture energy, and a >100-fold increase in fatigue life (56–58).

We have shown that Lrp5 function is required for the osteogenic response to mechanical loading. We do not yet know whether agents such as LiCl, which can activate canonical Wnt

signaling downstream of the receptor, can restore mechanoresponsiveness in patients with OPPG. Nor do we know whether other approaches to increase Lrp5 signaling in healthy individuals can enhance the response of the skeleton to exercise. Overexpression of the wild-type LRP5 receptor in mice (using a collagen I promoter fragment) did improve mechanical properties of bone, but it remains to be determined whether overexpression mediated its effect by enhancing load-induced bone gain (12). Responding to mechanotransduction is unlikely to be the sole function of Lrp5 in the skeleton. Canonical Wnt signaling has recently been demonstrated to enable marrow stromal cells to differentiate toward the osteoblast lineage, rather than other cell fates (59–61) and to alter the expression in mature osteoblasts of secreted regulators of osteoclast differentiation. Consistent with these additional functions, the administration of LiCl to Lrp5 mutant mice decreases marrow adiposity, whereas increasing trabecular bone volume (20).

We observed sex-related differences in the severity of the phenotype in Lrp5 mutant mice. Lrp5^{-/-} females exhibited a more mild phenotype in terms of BMC, structure (I_p , BV/TV), and mechanical properties (F_u , stiffness, work to failure) than their male counterparts. For some measurements, the phenotype was twice as severe in males. The reason for these disparities between the sexes is unclear, particularly in light of the known autosomal mode of transmission for OPPG. One potential explanation receiving increasing attention is the link between signaling in the estrogen and Wnt pathways, which appear to participate in considerable cross-talk. For example, transgenic mice expressing Wnt 10b are resistant to ovariectomy induced bone loss (59). Furthermore, estrogen receptor α (62) and androgen receptors (63, 64) interact functionally with β -catenin *in vivo*. If enhanced estrogen signaling in females is providing some osteo-protective effects from the loss of Lrp5 signaling, modulating that interaction pharmacologically could prove to be a useful target for OPPG patients.

In conclusion, Lrp5 appears to be a potent regulator of bone mass, size, and strength. One of the main mechanisms of action for the receptor in bone is through mechanical signaling, but not PTH signaling. Our data indicate that Lrp5 is a late-acting mediator in the osteogenic response to mechanical loading, suggesting that skeletal fragility in individuals afflicted with OPPG might be related to inadequate processing of signals derived from mechanical stimulation. In addition, intermittent PTH might be an effective treatment for improving bone mass in these patients.

Acknowledgments—We thank Andrea Paris for animal care, Jean Bao and Erin Hatt for assistance with uCT scanning, Dr. Shigeo Tanaka for technical assistance in loading device, and Dr. Keith Condon for assistance with tissue processing.

REFERENCES

- He, X., Semenov, M., Tamai, K., and Zeng, X. (2004) *Development* **131**, 1663–1677
- Gong, Y., Slee, R. B., Fukai, N., Rawadi, G., Roman-Roman, S., Reginato, A. M., Wang, H., Cundy, T., Glorieux, F. H., Lev, D., Zacharin, M., Oexle, K., Marcelino, J., Suwairi, W., Heeger, S., Sabatakos, G., Apte, S., Adkins, W. N., Allgrove, J., Arslan-Kirchner, M., Batch, J. A., Beighton, P., Black,

- G. C., Boles, R. G., Boon, L. M., Borrone, C., Brunner, H. G., Carle, G. F., Dallapiccola, B., De Paepe, A., Floege, B., Halfhide, M. L., Hall, B., Hennekam, R. C., Hirose, T., Jans, A., Juppner, H., Kim, C. A., Keppler-Noreuil, K., Kohlschuetter, A., LaCombe, D., Lambert, M., Lemyre, E., Letteboer, T., Peltonen, L., Ramesar, R. S., Romanengo, M., Somer, H., Steichen-Gersdorf, E., Steinmann, B., Sullivan, B., Superti-Furga, A., Swoboda, W., van den Boogaard, M. J., Van Hul, W., Viikula, M., Votruba, M., Zabel, B., Garcia, T., Baron, R., Olsen, B. R., and Warman, M. L. (2001) *Cell* **107**, 513–523
3. Boyden, L. M., Mao, J., Belsky, J., Mitzner, L., Farhi, A., Mitnick, M. A., Wu, D., Insogna, K., and Lifton, R. P. (2002) *N. Engl. J. Med.* **346**, 1513–1521
 4. Li, X., Zhang, Y., Kang, H., Liu, W., Liu, P., Zhang, J., Harris, S. E., and Wu, D. (2005) *J. Biol. Chem.* **280**, 19883–19887
 5. Ai, M., Holmen, S. L., Van Hul, W., Williams, B. O., and Warman, M. L. (2005) *Mol. Cell. Biol.* **25**, 4946–4955
 6. Johnson, M. L., Gong, G., Kimberling, W., Recker, S. M., Kimmel, D. B., and Recker, R. R. (1997) *Am. J. Hum. Genet.* **60**, 1326–1332
 7. Little, R. D., Carulli, J. P., Del Mastro, R. G., Dupuis, J., Osborne, M., Folz, C., Manning, S. P., Swain, P. M., Zhao, S. C., Eustace, B., Lappe, M. M., Spitzer, L., Zweier, S., Braunschweiger, K., Benchekroun, Y., Hu, X., Adair, R., Chee, L., FitzGerald, M. G., Tulig, C., Caruso, A., Tzelas, N., Bawa, A., Franklin, B., McGuire, S., Nogues, X., Gong, G., Allen, K. M., Anisowicz, A., Morales, A. J., Lomedico, P. T., Recker, S. M., Van Eerdewegh, P., Recker, R. R., and Johnson, M. L. (2002) *Am. J. Hum. Genet.* **70**, 11–19
 8. Van Wesenbeeck, L., Cleiren, E., Gram, J., Beals, R. K., Benichou, O., Scopelliti, D., Key, L., Renton, T., Bartels, C., Gong, Y., Warman, M. L., De Verneuil, M. C., Bollerslev, J., and Van Hul, W. (2003) *Am. J. Hum. Genet.* **72**, 763–771
 9. Fujino, T., Asaba, H., Kang, M. J., Ikeda, Y., Sone, H., Takada, S., Kim, D. H., Ioka, R. X., Ono, M., Tomoyori, H., Okubo, M., Murase, T., Kamataki, A., Yamamoto, J., Magoori, K., Takahashi, S., Miyamoto, Y., Oishi, H., Nose, M., Okazaki, M., Usui, S., Imaizumi, K., Yanagisawa, M., Sakai, J., and Yamamoto, T. T. (2003) *Proc. Natl. Acad. Sci. U. S. A.* **100**, 229–234
 10. Kato, M., Patel, M. S., Levasseur, R., Lobov, I., Chang, B. H., Glass, D. A., 2nd, Hartmann, C., Li, L., Hwang, T. H., Brayton, C. F., Lang, R. A., Karsenty, G., and Chan, L. (2002) *J. Cell Biol.* **157**, 303–314
 11. Iwaniec, U. T., Liu, G., Arzaga, R. R., Donovan, L. M., Brommage, R., and Wronski, T. J. (2004) *J. Bone Miner. Res.* **19**, Suppl. 1, S18
 12. Babij, P., Zhao, W., Small, C., Kharode, Y., Yaworsky, P. J., Bouxsein, M. L., Reddy, P. S., Bodine, P. V., Robinson, J. A., Bhat, B., Marzolf, J., Moran, R. A., and Bex, F. (2003) *J. Bone Miner. Res.* **18**, 960–974
 13. Bikle, D. D., Halloran, B. P., Cone, C. M., Globus, R. K., and Morey-Holton, E. (1987) *Endocrinology* **120**, 678–684
 14. David, V., Laroche, N., Boudignon, B., Lafage-Proust, M. H., Alexandre, C., Ruegsegger, P., and Vico, L. (2003) *J. Bone Miner. Res.* **18**, 1622–1631
 15. Jaworski, Z. F. G., Liskova-Kiar, M., and Uhthoff, H. K. (1980) *J. Bone Joint Surg.* **62-B**, 104–110
 16. Uhthoff, H. K., and Jaworski, Z. F. G. (1978) *J. Bone Joint Surg.* **60**, 420–429
 17. Brude, E., and Stoss, H. (1986) *7th International Congress on Human Genetics*, p. 35, Berlin
 18. Norvell, S. M., Alvarez, M., Bidwell, J., and Pavalko, F. M. (2005) *Calcif. Tissue Int.* **75**, 396–404
 19. Hens, J. R., Wilson, K. M., Dann, P., Chen, X., Horowitz, M. C., and Wysolmerski, J. J. (2005) *J. Bone Miner. Res.* **20**, 1103–1113
 20. Clément-Lacroix, P., Ai, M., Morvan, F., Roman-Roman, S., Vayssiére, B., Belleville, C., Estrera, K., Warman, M. L., Baron, R., and Rawadi, G. (2006) *Proc. Natl. Acad. Sci. U. S. A.* **102**, 17406–17411
 21. Kalajzic, I., Kalajzic, Z., Kaliterna, M., Gronowicz, G., Clark, S. H., Lichtler, A. C., and Rowe, D. (2002) *J. Bone Miner. Res.* **17**, 15–25
 22. Turner, C. H., Hsieh, Y. F., Muller, R., Bouxsein, M. L., Rosen, C. J., McCrann, M. E., Donahue, L. R., and Beamer, W. G. (2001) *J. Bone Miner. Res.* **16**, 206–213
 23. Turner, C. H., and Burr, D. B. (1993) *Bone* **14**, 595–608
 24. Torrance, A. G., Mosley, J. R., Suswillo, R. F., and Lanyon, L. E. (1994) *Calcif. Tissue Int.* **54**, 241–247
 25. Tanaka, S. M., Alam, I. M., and Turner, C. H. (2003) *FASEB J.* **17**, 313–314
 26. Robling, A. G., and Turner, C. H. (2002) *Bone* **31**, 562–569
 27. Parfitt, A. M., Drezner, M. K., Glorieux, F. H., Kanis, J. A., Malluche, H., Meunier, P. J., Ott, S. M., and Recker, R. R. (1987) *J. Bone Miner. Res.* **2**, 595–610
 28. Frangos, J. A., Eskin, S. G., McIntire, L. V., and Ives, C. L. (1985) *Science* **227**, 1477–1479
 29. Wolf, G., Schmidt, W., and Schunzel, G. (1980) *Acta Biol. Med. Ger.* **39**, 1243–1245
 30. Hsieh, Y. F., Robling, A. G., Ambrosius, W. T., Burr, D. B., and Turner, C. H. (2001) *J. Bone Miner. Res.* **16**, 2291–2297
 31. Gere, J. M., and Timoshenko, S. P. (1990) *Mechanics of Materials*, 3 Ed., PWS-Kent, Boston
 32. Boppert, M. D., Kimmel, D. B., Yee, J. A., and Cullen, D. M. (1998) *Bone* **23**, 409–415
 33. Turner, C. H., Owan, I., Alvey, T., Hulman, J., and Hock, J. M. (1998) *Bone* **22**, 463–469
 34. Genetos, D. C., Geist, D. J., Liu, D., Donahue, H. J., and Duncan, R. L. (2005) *J. Bone Miner. Res.* **20**, 41–49
 35. You, J., Jacobs, C. R., Steinberg, T. H., and Donahue, H. J. (2002) *J. Biol. Chem.* **277**, 48724–48729
 36. Harell, A., Dekel, S., and Binderman, I. (1977) *Calcif. Tissue Res.* **22**, (suppl.) 202–207
 37. Somjen, D., Binderman, I., Berger, E., and Harell, A. (1980) *Biochim. Biophys. Acta* **627**, 91–100
 38. Yeh, C. K., and Rodan, G. A. (1984) *Calcif. Tissue Int.* **36**, Suppl. 1, S67–S71
 39. Wadhwa, S., Godwin, S. L., Peterson, D. R., Epstein, M. A., Raisz, L. G., and Pilbeam, C. C. (2002) *J. Bone Miner. Res.* **17**, 266–274
 40. You, J., Reilly, G. C., Zhen, X., Yellowley, C. E., Chen, Q., Donahue, H. J., and Jacobs, C. R. (2001) *J. Biol. Chem.* **276**, 13365–13371
 41. Miles, R. R., Turner, C. H., Santerre, R., Tu, Y., McClelland, P., Argot, J., DeHoff, B. S., Mundy, C. W., Rosteck, P. R., Jr., Bidwell, J., Sluka, J. P., Hock, J., and Onyia, J. E. (1998) *J. Cell Biochem.* **68**, 355–365
 42. Raab-Cullen, D. M., Thiede, M. A., Petersen, D. N., Kimmel, D. B., and Recker, R. R. (1994) *Calcif. Tissue Int.* **55**, 473–478
 43. Owan, I., Burr, D. B., Turner, C. H., Qiu, J., Tu, Y., Onyia, J. E., and Duncan, R. L. (1997) *Am. J. Physiol.* **273**, C810–C815
 44. Toma, C. D., Ashkar, S., Gray, M. L., Schaffer, J. L., and Gerstenfeld, L. C. (1997) *J. Bone Miner. Res.* **12**, 1626–1636
 45. You, J., Yellowley, C. E., Donahue, H. J., Zhang, Y., Chen, Q., and Jacobs, C. R. (2000) *J. Biomech. Eng.* **122**, 387–393
 46. Kulkarni, N. H., Halladay, D. L., Miles, R. R., Gilbert, L. M., Frolik, C. A., Galvin, R. J., Martin, T. J., Gillespie, M. T., and Onyia, J. E. (2005) *J. Cell Biochem.* **95**, 1178–1190
 47. Holmen, S. L., Giambernardi, T. A., Zylstra, C. R., Buckner-Berghuis, B. D., Resau, J. H., Hess, J. F., Glatt, V., Bouxsein, M. L., Ai, M., Warman, M. L., and Williams, B. O. (2004) *J. Bone Miner. Res.* **19**, 2033–2040
 48. Yao, G. Q., Wu, J. J., Troiano, N., Bartkiewicz, M., Sun, B. H., and Insogna, K. (2005) *J. Bone Miner. Res.* **20**, Suppl. 1, S48
 49. Wang, Y., Nishida, S., Burghardt, A., ElAlieh, H. Z., Majumdar, S., Halloran, B. P., Clemens, T. L., and Bikle, D. D. (2004) *J. Bone Miner. Res.* **19**, Suppl. 1, S106
 50. Cullen, D. M., Akhter, M. P., Johnson, M. L., Morgan, S., and Recker, R. R. (2004) *J. Bone Miner. Res.* **19**, Suppl. 1, S396
 51. Kreke, M. R., Huckle, W. R., and Goldstein, A. S. (2005) *Bone* **36**, 1047–1055
 52. Li, Y. J., Batra, N. N., You, L., Meier, S. C., Coe, I. A., Yellowley, C. E., and Jacobs, C. R. (2004) *J. Orthop. Res.* **22**, 1283–1289
 53. Tanaka, S. M., Sun, H. B., Roeder, R. K., Burr, D. B., Turner, C. H., and Yokota, H. (2005) *Calcif. Tissue Int.* **76**, 261–271
 54. Rawlinson, S. C., Mohan, S., Baylink, D. J., and Lanyon, L. E. (1993) *Calcif. Tissue Int.* **53**, 324–329
 55. Pitsillides, A. A., Rawlinson, S. C., Suswillo, R. F., Bourrin, S., Zaman, G., and Lanyon, L. E. (1995) *FASEB J.* **9**, 1614–1622
 56. Robling, A. G., Hinant, F. M., Burr, D. B., and Turner, C. H. (2002) *Med. Sci. Sports Exer.* **34**, 196–202
 57. Robling, A. G., Hinant, F. M., Burr, D. B., and Turner, C. H. (2002) *J. Bone Miner. Res.* **17**, 1545–1554
 58. Warden, S. J., Hurst, J. A., Sanders, M. S., Turner, C. H., Burr, D. B., and Li, J. (2005) *J. Bone Miner. Res.* **20**, 809–816

59. Bennett, C. N., Longo, K. A., Wright, W. S., Suva, L. J., Lane, T. F., Hankenson, K. D., and MacDougald, O. A. (2005) *Proc. Natl. Acad. Sci. U. S. A.* **102**, 3324–3329
60. Gregory, C. A., Gunn, W. G., Reyes, E., Smolarz, A. J., Munoz, J., Spees, J. L., and Prockop, D. J. (2005) *Ann. N. Y. Acad. Sci.* **1049**, 97–106
61. Nuttall, M. E., and Gimble, J. M. (2004) *Curr. Opin. Pharmacol.* **4**, 290–294
62. Kouzmenko, A. P., Takeyama, K., Ito, S., Furutani, T., Sawatsubashi, S., Maki, A., Suzuki, E., Kawasaki, Y., Akiyama, T., Tabata, T., and Kato, S. (2004) *J. Biol. Chem.* **279**, 40255–40258
63. Pawlowski, J. E., Ertel, J. R., Allen, M. P., Xu, M., Butler, C., Wilson, E. M., and Wierman, M. E. (2002) *J. Biol. Chem.* **277**, 20702–20710
64. Yang, F., Li, X., Sharma, M., Sasaki, C. Y., Longo, D. L., Lim, B., and Sun, Z. (2002) *J. Biol. Chem.* **277**, 11336–11344
65. Rawlinson, S. C., el-Haj, A. J., Minter, S. L., Tavares, I. A., Bennett, A., and Lanyon, L. E. (1991) *J. Bone Miner. Res.* **6**, 1345–1351